Published in final edited form as:

IEEE Trans Ultrason Ferroelectr Freq Control. 2021 September ; 68(9): 2917–2929. doi:10.1109/TUFFC.2021.3068113.

Transcranial MR-guided Histotripsy System

Ning Lu [Student Member, IEEE],
Department of Biomedical Engineering, University of Michigan, Ann Arbor, MI 48109 USA

Timothy L. Hall,
Department of Biomedical Engineering, University of Michigan, Ann Arbor, MI 48109 USA

Dave Choi,
Department of Biomedical Engineering, University of Michigan, Ann Arbor, MI 48109 USA

Dinank Gupta,
Department of Biomedical Engineering, University of Michigan, Ann Arbor, MI 48109 USA

Badih J. Daou,
Department of Neurosurgery, University of Michigan, Ann Arbor, MI 48109 USA

Jonathan R. Sukovich,
Department of Biomedical Engineering, University of Michigan, Ann Arbor, MI 48109 USA

Adam Fox,
Department of Biomedical Engineering, University of Michigan, Ann Arbor, MI 48109 USA

Tyler I. Gerhardson,
currently with Histosonics Inc., Ann Arbor, MI 48103 USA. He was with the Department of Biomedical Engineering, University of Michigan, Ann Arbor, MI 48109 USA when this work was done.

Aditya S. Pandey,
Department of Neurosurgery, University of Michigan, Ann Arbor, MI 48109 USA

Douglas C. Noll [Senior Member, IEEE],
Department of Biomedical Engineering, University of Michigan, Ann Arbor, MI 48109 USA

Zhen Xu [Member, IEEE]
Department of Biomedical Engineering, University of Michigan, Ann Arbor, MI 48109 USA

Abstract

Histotripsy has been previously shown to treat a wide range of locations through excised human skulls in vitro. In this paper, a transcranial magnetic resonance (MR)-guided histotripsy (tcMRgHt) system was developed, characterized, and tested in the in vivo pig brain through an excised human skull. A 700-kHz, 128-element MR-compatible phased-array ultrasound transducer

ninglu@umich.edu .

DISCLOSURES

Drs. Zhen Xu, Timothy Hall, and Tyler Gerhardson have financial and/or other relationships with HistoSonics Inc.

with a focal depth of 15 cm was designed and fabricated in-house. Support structures were also constructed to facilitate transcranial treatment. The tcMRgHt array was acoustically characterized with a peak negative pressure up to 137 MPa in free field, 72 MPa through an excised human skull with aberration correction, and 48.4 MPa without aberration correction. The electronic focal steering range through the skull was 33.5 mm laterally and 50 mm axially, where peak negative pressure above the 26 MPa cavitation intrinsic threshold can be achieved. The MR-compatibility of the tcMRgHt system was assessed quantitatively using SNR, B0 field map, and B1 field map in a clinical 3T MRI scanner. Transcranial treatment using electronic focal steering was validated in red blood cell phantoms and in vivo pig brain through an excised human skull. In two pigs, targeted cerebral tissue was successfully treated through the human skull as confirmed by MRI. Excessive bleeding or edema was not observed in the peri-target zones by the time of pig euthanasia. These results demonstrated the feasibility of using this preclinical tcMRgHt system for in vivo transcranial treatment in a swine model.

Keywords

Histotripsy; magnetic resonance imaging (MRI); transcranial treatment; therapeutic ultrasound

I. Introduction

TRANSCRANIAL magnetic resonance-guided focused ultrasound (tcMRgFUS) has been investigated for non-invasive ablation to treat neurological-disorders and brain tumors [1–9]. Guided by MRI, ultrasound is applied from outside the skull and focused on the target brain tissue to produce thermal ablation, while the surrounding brain and the skull remain intact. As a new non-invasive neurosurgical tool, tcMRgFUS has received enthusiastic responses from the clinical community. Commercial tcMRgFUS thermal ablation systems have been approved by the U.S. Food and Drug Administration (FDA) to treat essential tremors by ablating a single focal volume within the central nervous system [2–4]. Laboratory investigation and clinical trials on using tcMRgFUS to treat Parkinson's diseases are also currently ongoing [10],[11]. However, due to overheating of the skull, which is highly absorptive and reflective of ultrasound, it is challenging for tcMRgFUS to treat locations within 2 cm from the skull surface, rendering inoperable up to ~90% of the cortex where brain tumors often reside [8],[9],[12],[13]. Moreover, the peri-target heating due to the ultrasound absorption in surrounding tissue limits the treatment rate of tcMRgFUS for large targets [9],[12], resulting in a long treatment time that may be unbearable for patients with large tumors.

Unlike tcMRgFUS that relies on heating produced by continuous sonication, histotripsy uses short (several μsec), high-pressure ultrasound pulses (>26 MPa) to generate focused cavitation bubbles, which mechanically fractionate and liquefy the target tissue into acellular homogenate [14–16]. As the damage generated by histotripsy is confined to only the regions where the pressure exceeds the intrinsic threshold for nucleation, histotripsy has shown to be particularly robust even in situations where severe aberrations are introduced by heterogeneous mediums such as the human skull [17], [18]. With long cooling times between pulses (ultrasound duty cycle <0.1%), transcranial histotripsy reduces heating of the

skull and surrounding tissue while effectively ablating the target tissue. Gerhardson *et al.* have shown that applied through excised human skulls, histotripsy can liquefy up to 40 ml of a clot within 20 minutes (corresponding to a treatment rate of 2 cm^3/minute) in varying depth from the skull base to 5 mm from the inner skull surface, keeping the temperature increase in the skull <4°C [19]. As histotripsy mechanically disrupts the target tissue, there was a concern that histotripsy may cause excessive hemorrhage or edema in the brain. An initial *in vivo* study by Sukovich *et al.* showed that cerebral lesions can be generated in the normal pig brain without excessive bleeding in the acute and subacute phases after treatment [21]. These preliminary results suggested the potential of using histotripsy for non-invasive transcranial treatment.

Since histotripsy-generated cavitation can be visualized by ultrasound imaging, histotripsy treatment is typically guided by ultrasound imaging [22], [23]. However, transcranial ultrasound imaging remains a challenge without contrast agents. To develop transcranial histotripsy techniques for non-invasive brain applications, transcranial MR-guided histotripsy (tcMRgHt) is necessary to provide MR brain scans for targeting and monitoring to ensure treatment efficacy and accuracy. Previous studies by Allen *et al.* have shown that histotripsy-induced cavitation and tissue fractionation can be visualized on MRI with specialized MRI sequences [24], [25].

Here, the first preclinical tcMRgHt system is designed and fabricated. Although the feasibility of transcranial histotripsy [17–20] and MRI guidance [24],[25] have been shown separately, developing an integrated tcMRgHt system presents a substantial technical challenge. The design of the tcMRgHt system is different than general histotripsy systems mainly in three aspects. 1) The system is required to be MR-safe with the minimal mass of metal, and the cables connecting the transducer elements to the driving electronics should be long enough to ensure the driving electronics and power supplies are outside the 0.5 mT line, often conveniently in the MR control room separately from the scanner room. 2) Sufficient MR image quality is required with the tcMRgHt system in the MR scanner for treatment targeting and monitoring [26], [27]. Therefore, noise and artifacts introduced by the histotripsy system need to be mitigated by appropriate separation and filtering of the electronics from MRI receive coils and possibly careful synchronization between the histotripsy pulses and MRI pulse sequences. 3) This tcMRgHt system was designed to perform preclinical in vivo studies on human-scale pigs through an excised human skull. Non-metallic mechanical fixtures were thus designed and fabricated specifically for the geometry of porcine heads. Besides, our design goal includes sufficient headroom of ultrasound pressure and a large electronic focal steering range to maximize the treatment efficiency for volume targets in the brain. These features all need to be taken into consideration and carefully addressed when developing the tcMRgHt system.

In this paper, we present the design and construction of the first preclinical tcMRgHt system, which includes a 700-kHz, 128-element MR-compatible ultrasound phased array. The tcMRgHt system is acoustically characterized by focal pressure output, beam profiles, and electronic steering profiles. We also quantitatively assess the MR-compatibility of the tcMRgHt system by the signal-to-noise ratio (SNR), B0 field map, and B1 field map acquired using gradient echo sequences with the tcMRgHt system in a clinical 3T MRI

scanner. Finally, the feasibility of using tcMRgHt to treat a volume target using electronic focal steering was tested in a red blood cell agarose phantom, and the feasibility of using tcMRgHt for in vivo transcranial treatment was demonstrated in the brain of two pigs through an excised human skull.

II. Methods

A. Histotripsy system design and fabrication

1) Array design: The structural design of the MR-compatible transcranial transducer was based on previously developed hemispherical arrays in house and commercial tcMRgFUS arrays, both with a radius of 150 mm. The center frequency of 700 kHz was chosen based on a thorough study taking into account the skull transmission, aberration, focal gain, electronic steerability, cost, and electrical component limitations [28]. The full hemispherical array consists of 360 17-mm square modules, resulting in a surface area packing density of 74% compared to 57% for a prior 500 kHz 256-element design [18]. The increased frequency and packing density of this new design enabled a significantly higher power output and electronic steering range above the intrinsic cavitation threshold through the human skull.

The initial motivation for this tcMRgHt system is to enable preclinical studies in the in vivo porcine brain through an excised human skull, which was a previously used model for the preclinical tcMRgFUS studies [6], [29]–[31]. As the pig skull is much thicker and flatter compared to the human and leads to excessive attenuation, a craniotomy was first performed to create a 60 mm diameter opening through the pig skull to access the pig brain. An excised human calvarium was then placed over this acoustic window. With this experimental setup, approximately 2/3 outer portion of the 360-element array aperture would be blocked by the remaining pig skull. The 360-element hemispherical array was initially designed for human use. Thus, for the porcine study, we used the 360-element array scaffold but only populated the inner 1/3 portion of the full array scaffold for this tcMRgHt system, resulting in an effective aperture of the array truncated to the inner 128-elements with an effective f-number (focal distance/ aperture diameter) of 0.74 as demonstrated in Fig. 1.

2) Transducer fabrication: The 128-element array was fabricated by mounting 128 individual transducer modules to a plastic scaffold. Each module was constructed from a porous PZT material (PZ36, Meggitt A/S, Denmark) in a 3D-printed housing. Fig. 2 shows the cross-section of the transducer module design and a photo of a single unit. Two matching layers, Somos PerFORM (5 MRayl) and laser-sintered polyacrylamide (2 MRayl), with the thickness of a quarter-wavelength, were used to provide a smoother gradient for acoustic impedance than a single matching layer so that acoustic energy transmits more efficiently from the PZT to the medium. The backing end of the module was filled with epoxy (314 Resin & 143 Hardener, TAP Plastics Inc., San Leandro, CA, USA) to ensure a water-tight seal around the PZT element and allowed the module to be fully submerged. O-ring retaining grooves on the outside of the housing allowed the modules to be secured to the sockets on the array scaffold via an easily removable O-ring and to be easily replaced individually if any module is damaged, thus keeping maintenance costs low. Electrical

connections from driving circuits to the individual modules were made via micro-coaxial cable (9432 WH033, Alpha Wire, USA) and high-density connectors (DL2-96, ITT Cannon LLC, Irvine, CA, USA). The coaxial cables were rigidly soldered to the transducer element on one end and remained connected to the tcMRgHt array for all experiments. 3D-printed strain reliefs were attached around the electrical connection to provide tension relief for the cables.

3) Driving electronics: Driving electronics were built in-house to produce 3.5 kV peak amplitude and 20 A to drive each transducer element with microsecond length (1-cycle at 700 kHz) ultrasound pulses at a very high focal pressure for histotripsy (Fig. 2c). A field-programmable gate array (FPGA) controlled via USB by MATLAB (The MathWorks Inc., Natick, MA, USA) interface allowed arbitrary pulsing of modules with 10 ns timing precision. Programmable trigger signals can be fed from the MR scanner or sent to the scanner to synchronize the histotripsy pulse with imaging sequences. 1-cycle pulse length was used to generate cavitation, as the short pulse length has been demonstrated to successfully eliminate the formation of standing waves in the brain [32]. Driven by the 1-cycle pulse with 3.5 kV peak amplitude, a single transducer element produced a peak negative pressure (P-) of 1.36 MPa at 150 mm in the free field, as shown in Fig. 2d.

4) Compatibility with MRI system: The new array adhered to standards for an MR conditional device to ensure patient safety and good imaging quality. All metallic components (fasteners, cables, etc.) consisted of non-ferrous materials. With sintered silver electrode PZT crystals, nylon scaffold, and 3D printed housing and matching layers, this design minimized the mass of metal to maintain good MR image quality. The modular construction technique inherently resulted in a segmented ground plane, which has been shown to yield better MR image quality compared to continuous plane design [33], as it allows radiofrequency (RF) magnetic field penetration through spaces between the ground plane segments. The driving electronics were placed in an adjacent control room outside of the MR scanner room, and the coaxial cables were fed through the waveguide penetrations of the panel between the control room and scanner room for shielding. All experiments were conducted with a clinical 3T MRI scanner (Discovery MR750, GE Healthcare, Milwaukee, WI, USA). The evaluation of MR image quality with the tcMRgHt system in the scanner is described in Section II.C and III.B.

5) Support structures: To facilitate the in-vivo transcranial pig treatment, support structures were required to 1) stably mount the transducer array onto the MR scanner bed, 2) firmly fix an excised human calvarium at a set location and orientation, and 3) position pig heads of a range of sizes at a desired location and orientation. The assembly of the transducer and all its support structures is illustrated in Fig. 3. The bottom of the array frame was contoured to mate with the scanner to keep the array stable on the MR bed. The whole assembly was placed in a cylindrical waterproof canvas bag and immersed in the coupling medium (water for acoustic characterization, saline solution for MR-compatibility testing and in vivo treatment) during the experiments.

The calvarium holder was designed to be mounted to the unpopulated spaces on the scaffold and was shaped to avoid interfering with the ultrasound propagation path from any of the

populated transducer elements at the bottom of the scaffold. To accommodate a variety of calvarium sizes and shapes, adjustable screws and clamps were used to fix the skull around its perimeter. Fiducial markers were also attached to the skull holder to quickly identify the geometric focus of the transducer array from an MR image and assist in targeting.

Neck and snout holders were designed based on empirical measurements from two pigs of representative size (27 kgs and 32 kgs juveniles) for in vivo histotripsy treatment. The heights of these holders were arranged to hold the pig head level and at an optimal angle to provide the best acoustic window through the craniotomy opening. Adjustable Velcro straps fitted to the holders were used to secure the pig's neck and snout during the experiments. These straps also provided some level of vertical adjustment for pig head positioning. Additionally, the neck and snout holders were fixed to a series of slots on a top plate that was fabricated using acetal plastic. These slots allowed adjustment to accommodate different pig head lengths as well as forward-to-rear and left-to-right positioning of the pig head. The plates also provided support for the MR surface coil pads, reducing any chances for them to shift or tilt during the image acquisition. A spirit level was mounted on top of the histotripsy array to check the horizontal level.

B. Transcranial acoustic characterization

The fully assembled MR-compatible histotripsy array was acoustically characterized using the focal pressure, the size of the focal zone, and the capability of electronic focal steering. For transcranial ultrasound therapy, the skull in the ultrasound pathway causes significant attenuation and aberration to the ultrasound beam due to its non-uniform thickness and composition [34], [35]. The high attenuation and strong phase aberrations introduced by the calvarium can distort the shape of the pressure field and decrease its amplitude at the target location, thereby limiting the treatment's effectiveness. Therefore, to quantify the pressure loss due to the skull and how much of this loss can be recovered by refocusing the beam, measurements were obtained in three experimental settings: (a) in the free field; (b) through an excised human calvarium without aberration correction; (c) through the calvarium with aberration correction. All measurements were obtained in degassed water at room temperature.

1) Skull preparation: An excised human calvarium was obtained from the University of Michigan Anatomical Donations Program and used for the phantom treatment and in vivo pig treatment. The calvarium was de-fleshed and cleaned after extraction and kept in either water or a 5% bleach-water solution thereafter. The bleach was added to prevent the growth of algae or bacteria on the surface of the calvarium and the walls of the storage container. Before experiments, the calvarium was degassed in water inside a vacuum chamber for a minimum of 6 hours. During the experiments, the calvarium was held by the skull holder and fixed at a set location and orientation throughout all experiments including acoustic characterization, MRI testing, and pig treatment. The major dimensions of the calvarium were 158 mm on the long axis (maximum front-to-back length on the exterior surface), 139 mm on the short axis (maximum end-to-end length on the exterior surface), and 56 mm in depth (maximum distance from the interior surface to the cut plane of the skull). The minimal and maximal thicknesses of the calvarium were 2.5 mm and 8.5 mm, respectively.

2) Focal pressure: To characterize the focal pressure of the tcMRgHt transducer array, the P- at the geometric focus was directly measured in free field and through the calvarium using a fiber-optic hydrophone built in-house [36] up to 15 MPa with all elements pulsed simultaneously. At P- higher than 15 MPa, the pressure could not be measured directly due to instantaneous cavitation generation at the fiber tip. In this case, the focal pressure was estimated by linear summation of the measured pressure using a calibrated bullet hydrophone (HGL-0085, Onda, Sunnyvale, CA, USA) from individual transducer elements, each driven at the highest driving voltage of 3.5 kV. This method of estimating pressures has been shown to agree well with direct pressure measurements at pressures up to and beyond the intrinsic threshold [37]. To compensate for the phase aberration induced by the skull, the waveforms from individual elements were aligned and the P- were summed to estimate the focal pressure through the skull with aberration correction, P_{TC+AC}. In comparison, the focal pressure through the skull without aberration correction, P_{TC}, was estimated by P- of the directly summed waveform from individual elements without alignment. The transmission rate through the skull was calculated as $p_{transmission} = \frac{P_{TC}}{P_{FF}} \times 100\%$, where P_{FF} is the focal pressure in the free field. The percent of pressure recovered by aberration correction, $p_{recovered}$, was calculated by dividing the pressure difference between P_{TC+AC} and P_{TC} by the pressure difference between P_{FF} and P_{TC}, given by, $p_{recovered} = (P_{TC+AC} - P_{TC})/(P_{FF} - P_{TC}) \times 100\%$.

3) Beam profiles: To characterize the dimensions of the focal zone, 1-D beam profiles along 3 axes were measured using a needle hydrophone (HNR-0500, Onda, Sunnyvale, CA, USA) at low pressure (i.e., <2 MPa) with a fixed driving voltage. The hydrophone was affixed to a motorized 3-D positioning system, centered at the geometric focus, and scanned ± 20 mm in 0.25-mm steps along the sagittal, coronal, and axial axes of the calvarium. To obtain beam profiles through the skull with aberration correction, waveforms from individual transducer elements were acquired and cross-correlated to a single reference channel. The associated correlation delays were then applied as offsets to the elements firing time to align the pulses at the focus. As the tcMRgHt system delivers 1-cycle pulses for intrinsic threshold histotripsy, beam profiles were all acquired in reference to P- at each hydrophone position. The focal size was determined as full width half maximum (FWHM) of the focal beam profile on three axes. It should be noted that we used $dB = 20log_{10}\left(\frac{P}{P_{\max}}\right)$ for all acoustic measurements in this paper, where P_{max} is the maximum P- that was measured in the field and P is the P- at other locations. Thus, −6 dB refers to merely half of the P_{max} and the FWHM corresponded to the distance between two locations where −6 dB was achieved on the profile.

4) Electronic focal steering range: To characterize the electronic focal steering range, the focal pressure as a function of electronic focal steering location was measured in free-field and through the calvarium. The array was steered in 0.25-mm steps across a ± 25-mm range of locations centered at the geometric focus in the sagittal, coronal and axial dimensions with a fixed driving voltage. For each electronic focal steering location, the 3-D positioner moved the needle hydrophone (HNR-0500, Onda, Sunnyvale, CA, USA)

to the steering location to record the pressure. The measurements were obtained at low pressure (<2 MPa) to avoid damaging the hydrophone. The steering profiles in the free field and through the calvarium without aberration correction were directly measured with all transducer elements pulsed simultaneously. For transcranial steering range with aberration correction, we measured waveforms from each element individually at the steering locations, calculated the phase difference between elements, corrected for the phase difference, and then summed the waveforms together to characterize the beam profile at each steered location, which effectively compensated for the aberration at the steering locations. Steering profiles on 3 axes were scaled to the focal pressure at a driving voltage of 3.5 kV (measured or estimated in the Focal pressure section) in each case correspondingly. The electronic steering range was characterized by the −6 dB range and the effective therapeutic range where >26 MPa can be generated, as the cavitation intrinsic threshold in brain tissue is 26 MPa [37], [38].

5) Lesion generation with electronic focal steering: To demonstrate transcranial histotripsy using electronic focal steering only, lesions were generated in a red blood cell (RBC) phantom through the human calvarium. The RBC phantom consisted of 2 layers of transparent agarose gel and a thin layer of gel with 5% bovine red blood cells in-between, as previously described by Maxwell *et al.*[39]. As the RBC-gel layer changed from translucent and red to colorless after the destruction of the RBC due to cavitation, the phantom provided a good contrast for visualizing cavitation damage. Lesions were generated in a sparse grid pattern (Fig. 8a) to show the precision of histotripsy ablation and in a continuous grid (Fig. 8b) to demonstrate volume treatment. The sparse grid treatment was applied through the calvarium without aberration correction. For the volume treatment, aberration correction was achieved by cross-correlating the individually acquired pressure waveforms from the hydrophone measurements to a single reference signal and applying the associated correlation delays as offsets to the elements' firing times to align the pulses at the focus. Two hundred histotripsy pulses were delivered to each steering location through the calvarium at a pulse repetition frequency (PRF) of 20 to 50 Hz. The tcMRgHt system was fired at a fixed acoustic power which provides P- of 48 MPa at the geometric focus of the array for both experiments.

C. MRI with histotripsy system

The MR-compatibility of the tcMRgHt system was evaluated by noise and artifacts induced by the experimental setup. The body coil of the MRI scanner was used for both transmission and receiving for studies in this section. Deionized water and degassed saline were used as the acoustic coupling medium from the histotripsy transcranial array through the excised human skull, for SNR measurement and field maps, respectively.

1) Signal-to-noise ratio (SNR): SNR has traditionally been presented as an important index of image quality in MR scans, which compares the level of the desired signal to the level of background noise. To understand the main source of noise in the tcMRgHt experimental configuration, we measured the SNR in the following five cases. For all five cases, one end of the cables was connected to the tcMRgHt array placed in the MR scanner, and the driving electronics were in the control room. (1) The cables were entirely left in

the scanner room, disconnected from the driving electronics in the control room. (2) The cables were passed through the waveguide penetration from the scanner room to the control room and remained unconnected to the driving electronics. (3) The cables were passed through the waveguide and connected to the driving electronics via high-density connectors and the electronics were powered up, but no ultrasound pulses were delivered. (4) The cables were passed through the waveguide and connected to the driving electronics via high-density connectors, and the ultrasound array was pulsed at 10 MPa below the cavitation intrinsic threshold at a PRF of 10 Hz. (5) The cables were passed through the waveguide and connected to the driving electronics, and the ultrasound array was pulsed at 48.4 MPa above the cavitation intrinsic threshold at a PRF of 10 Hz. A 2D spoiled gradient echo sequence was used for imaging with the following imaging parameters: TE = 10 ms, TR = 500 ms, flip angle = 30°, NEX = 2, grid size = 256 x 256 (re-sampled to 512 × 512), FOV=38 × 38 cm^2, slice thickness = 3 mm. The SNR for each case was calculated as $SNR = \mu/\sigma$, where μ was the mean of 100 × 70 voxels in focal region of the transducer and σ was the standard deviation of the 400 × 80 background voxels in the air above the tcMRgHt system, as labeled in Fig. 4.

2) B0 homogeneity: Field homogeneity refers to the uniformity of the magnetic field in the center of the scanner when no patient or phantom is present. The main magnetic field (B0) homogeneity is critical for MR image quality, as poor field homogeneity causes artifacts such as image distortions, blurring, and signal loss. Ideally, B0 should be homogeneous within a specified tolerance, and the remaining off-resonance effects can be mitigated by a shimming operation before the scan. However, the field may be further distorted by any wires, metal, or fringe fields in the immediate environment of the scanner.

To investigate the B0 homogeneity with the presence of the tcMRgHt system in the MR scanner, we measured the off-resonance in Hz as a B0 map from two scans with different echo times using a standard method [40], [41]. The mean and standard deviation of 60 × 25 voxels in the focal region of the histotripsy array were used as metrics for off-resonance induced by the tcMRgHt system. A 2D spoiled gradient echo sequence was used for imaging with the following imaging parameters: TE_1 = 10 ms, TE_2 = 12 ms, TR = 500 ms, flip angle = 30°, NEX = 1, grid size = 192 x 192 (re-sampled to 512 × 512), FOV=38 × 38 cm^2, slice thickness = 3 mm. An intensity-based binary mask shown as Fig. 9a was applied to the reconstructed B0 and B1 data to mask out the air-filled areas, as we are most interested in the field homogeneity within the transducer focal region.

3) B1 homogeneity: The RF field (B1) is applied perpendicular to the B0. For in vivo MRI at high field (>= 3 T), it is essential to consider the homogeneity of the B1 field. When exciting a large collection of spins, inhomogeneity in B1 results in non-uniform tipping of spins, leading to spatially varying image contrast and artifacts. The B1 field experienced by spins within the object is influenced by several factors including the distance from the RF transmit coil to the object, dielectric properties of the object, and factors related to the object size and RF wavelength.

To investigate the B1 homogeneity with the presence of the tcMRgHt system in the MR scanner, we measured the actual tip angle using the double angle method [42]. Since the

actual tip angle is proportional to the B1 magnitude, the mean and standard deviation of 60 × 25 voxels in the focal region were used as metrics for B1 inhomogeneity induced by the tcMRgHt system. A 2D spoiled gradient echo sequence was used for imaging with the following imaging parameters: TE = 10 ms, TR = 6 s, α_1 = 60°, α_2 = 120°, NEX = 1, grid size = 192 x 192 (re-sampled to 512 × 512), FOV=38 × 38 cm^2, slice thickness = 3 mm. Like B0 mapping, the intensity-based binary mask shown in Fig. 9a was also applied here to mask out the air-filled areas.

D. In vivo treatment: Pilot study on transcranial pig brain ablation

The feasibility of the tcMRgHt system was demonstrated in the in-vivo porcine brain through the excised human skull in two 27-37 kgs juvenile pigs. This study was approved by the Institutional Animal Care and Use Committee at the University of Michigan. The anesthetization and craniotomy procedures were performed at the University of Michigan animal surgery and operating room. For each pig, a 60 mm diameter circular region of the calvarium was surgically removed with the dura kept intact. After the craniotomy, the skin was sutured and sterile phosphate-buffered saline solution (0.9% sodium chloride, Hospira, Lake Forest, IL, USA) was injected under the skin flap to fill the vacant space. Pigs were recovered for two days before histotripsy treatment to allow the dissolution of any air trapped in the incision.

On the treatment day, the pigs were anesthetized and transferred to the Functional MRI lab. Vital signs were monitored through all procedures. The experimental setup in the MR scanner is shown in Fig.5. The tcMRgHt system was placed on the MRI bed and imaged by MRI before the treatment. The pig was placed supine on a v-tray with its head supported by the snout and neck holders. The pig head was positioned to the appropriate location and orientation to ensure the desired target in the brain lay within the electronic steering range for optimal treatment efficacy. The sound was coupled with degassed saline from the histotripsy transcranial array through the excised human skull, sutured skin, and dura into the pig brain.

Before the treatment, T2 and T2* images were taken as a reference for treatment outcome evaluation and used to locate the target via fiducial markers. Based on the fiducial markers on the array scaffold, the location of the array geometric focus was identified on the MR image, and the pig was moved to place the geometric focus of the array within the target volume. Then, an electronic focal steering pattern was created to cover a volume of target locations. For the first pig, a 3 × 3 × 3 mm volume was targeted by applying histotripsy to a grid of focal positions with a spacing of 1 mm on all 3 axes. A 6 × 6 × 3 mm volume was targeted in the second porcine brain, with a spacing of 1 mm on the x- and y-axis and a spacing of 1.5 mm on the z-axis. A previous intracranial study by Sukovich *et al.* [20] has shown that the degree of damage within the focal volumes was observed to increase with dose, with 10 pulses resulting in damage to 60% of the tissue within the focal volume and 50+ pulses resulting in damage ≥ 90% [21]. Therefore, with focal spacing smaller than the focal width resulting in some overlapping foci, we delivered 50 pulses to each focal location at a pulse repetition frequency of 10 Hz at a P_{max} of 48.4 MPa. Since it has been shown that compact targeted lesions can be generated through calvariums using histotripsy

without aberration correction when the pressure above the intrinsic threshold (P- = 26 MPa) is delivered to the target, and the goal of this section is just to demonstrate the feasibility of tcMRgHt, no aberration correction was applied for in vivo treatment to simplify the experimental procedure.

We used 10 cm DuoFLEX receive array coils (MR Instruments, Minneapolis, MN) to improve SNR over the pig brain. When the treatment was done, T2 and T2* images were acquired immediately after the treatment and 2~4 hours post-treatment before euthanizing the pig. T2-weighted MR images were chosen to show homogenized tissue and brain edema, whereas T2* images, as a measure of iron and hemosiderin in the brain, can demonstrate bleeding. The pig brain was then fixed in a 10% buffered formalin solution for 7 days and embedded in paraffin for histological analysis.

III. Results

A. Acoustic Characterization

1) Focal pressure: The maximal focal peak-negative pressure P- was estimated to be 137 MPa in the free field and 48.4 MPa through the skull without aberration correction, with a transmission rate $p_{transmission}$ of 35% through the skull. Estimated by the linear summation, the focal pressure through the skull with aberration correction was 72 MPa, recovering 27% of the pressure loss induced by the skull. Compared to the previously reported intrinsic cavitation threshold of 26 MPa in the brain tissue [37], [38], the achieved focal pressure provided sufficient acoustic power for transcranial treatment.

2) Beam profiles: 1-D beam profiles around the geometric focus were shown in Fig. 6 and summarized in Table 1. Phase distortion from the nonuniform thickness of the skull affected the beam profiles on all three axes, particularly in axial coordinates (X-axis), where the FWHM values increased 21% compared to the focal size in the free field from 1.9 mm to 2.3 mm. The focal beam was also found to be spatially shifted by 0.25 mm in X and Y coordinates. The aberration correction refocused the beam to produce smaller FWHM compared to the original beam in the free field on the Y and Z axes, but it only had a slight impact on the beam spatial distribution on X-axis.

3) Electronic focal steering range: The normalized peak-negative pressure as a function of electronic focal steering location along each axis was summarized in Table 1. As shown in Fig. 7, the −6 dB range in three cases remained similar with a range of 1.75 mm on the transverse plane, but the effective therapeutic range (where P->26 MPa can be achieved) decreased significantly through the skull than that in the free field, because the attenuation and aberration induced by the calvarium became prominent as the steering locations move further from the geometric focus. With aberration correction, such effects were mitigated, leading to a 47% increase and a 37% increase of the effective therapeutic range on the X and Y axes, respectively. As the aberration correction also focused the pressures on Z-axis and the effective therapeutic range without aberration correction was measured to be larger than 50 mm already, the steering profile with aberration correction was not shown in Fig.7. Besides, the steering range was found to be spatially shifted by 2 mm in the Y coordinate and 3 mm in the Z coordinate.

4) Lesion generation with electronic focal steering: The transcranial treatment using electronic focal steering was visualized using the RBC phantoms in Fig. 8. The size of lesions on the sparse circular pattern (Fig.8a) ranged from 0.6 mm to 2.3 mm due to the aberration and attenuation through the excised human skull, indicating the precision limits for transcranial histotripsy treatment. The 10-mm continuous square lesion in Fig. 8b demonstrated that the tcMRgHt system can treat volume targets using electronic focal steering through the excised human skull.

B. MRI with histotripsy system

1) SNR: The SNR from 5 experimental configurations was measured to be 143, 52, 50, 48, and 47, respectively. A factor of 2.75 drop in SNR was observed when the cables were passed through the waveguide penetration (comparing case 1 and case 2). Connecting the cables to the driving electronics (comparing case 2 and case 3) and applying the ultrasound pulses (comparing case 3 and case 4) led to a slight SNR decrease. When the ultrasound was applied, the acoustic pressure at the focus (above or below the cavitation threshold, comparing case 4 and case 5) had a negligible impact on SNR. These results indicated that the power status, the electrical excitation, and the acoustic pressure of the histotripsy array interfered negligibly with the MR scanner, thus enabling operating the MRI while delivering histotripsy treatment and offering good SNR for treatment evaluation.

2) B0 homogeneity: Fig. 9b shows the measured B0 map. Artifacts occurred locally at the ultrasound transducer elements and did not extend into surrounding areas. In the focal region of the histotripsy array, the mean and standard deviation of off-resonance were 16.3 Hz and 23.4 Hz respectively. Overall, the mean and standard deviation of off-resonance on the B0 map was −7.0 Hz and 44.8 Hz respectively, suggesting a sufficient B0 homogeneity with the tcMRgHt system in the scanner.

3) B1 homogeneity: Fig. 9c shows the measured tip angle map. Like the B0 map, artifacts occurred around the transducer elements but well-confined within the elements and array scaffold. Compared to the prescribed tip angle of 60°, over-tipping was shown in the central region of the image, coinciding with the effects previously seen in clinical human scans with the center being brighter than the edges [42]. In the focal region of the histotripsy array, the mean and standard deviation of tip angle were 69.1° and 16.0°, respectively. Overall, the mean and standard deviation on the B1 map with the mask was 58.9° and 12.9° separately, suggesting a sufficient B1 homogeneity with the tcMRgHt system in the scanner.

C. In vivo treatment

The tcMRgHt system was used to successfully generate ablation in the brain of two pigs through the excised human calvarium. T2-weighted MR images showed hyper-intense histotripsy ablation zones compared to the surrounding untreated tissue, as the cavitation generated by histotripsy liquefied the tissue (Fig. 10). These hyper-intense regions were confined within the targeted volume and did not demonstrate significant brain edema. T2* images, as a measure of iron and hemosiderin in the brain, demonstrated no excessive bleeding in peri-target zones post-treatment. Ablation zones in both pigs were identified in the deep brain region adjacent to the ventricles. The effective ablation zones were also

confirmed by histology, which revealed complete cellular disruption within the ablation zones and great correlation to the identified treatment zones on MRI.

IV. Discussion

The 128-element tcMRgHt system used in this study was specifically optimized for preclinical in vivo pig treatment. For human cadaver treatment or in real clinical cases, no craniotomy is needed as the ultrasound can propagate through the human skull. Therefore, to improve the treatment efficiency, a fully populated 360-element hemispherical histotripsy array will be used for cadaver and human studies. Such modification will also improve the precision of histotripsy treatment, as some of the off-target damage observed in the RBC phantom treatment might be attributable to the low F-number of the 128-element array.

One major improvement on this tcMRgHt array compared to previous histotripsy arrays was the use of the high-density connectors for connections from the array elements to the driving electronics. Getting rid of hundreds of separate connectors, this design was space-efficient and simplified the setup procedure for treatment in the MR scanner. Initially, the authors had concerns that the tight packing of the pins in the connector, coupled with the high driving voltages of the system, might result in electrical cross-talks between elements, which may lead to power loss when applying electronic focal steering. However, the amplitude of cross-talks at 700 kHz was quantified to be less than −54 dB compared to the actual driving amplitude, demonstrating the efficiency and robustness of this design.

The steering profiles suggested that the acoustic power decreased with the distance between the steering locations and the geometric focus. Applying aberration correction can increase the effective therapeutic steering range, as shown in Table 1 and Fig.7. However, for maximal acoustic efficiency, it is important to set the target tissue as close to the geometric focus of the histotripsy array as possible, which in reality often remains a major challenge when positioning the head, as observed during the in vivo pig treatment. Alternatively, a potential method to solve this issue would be to move the histotripsy array using an MR-conditional motorized positioner, with the location and orientation of the target tissue fixed during the treatment. To ensure the ultrasound beam strikes the skull with normal incidence, treatment planning software will be required along with the positioner to coregister the array with the subject’s head in real-time and visualize the beam so that we can deactivate the elements where the incident angles are greater than the critical angle, calculate the transmission efficiency, and then choose the optimal location and orientation.

For the in-vivo porcine treatment, hydrophone-based aberration correction was implemented to compensate for the phase variance introduced by the calvarium before the treatment to improve the efficiency of histotripsy treatment. This method did not take account of the aberration induced by the skin and brain tissue on the beam path. Besides, the invasiveness of inserting the hydrophone would also make it less favorable in clinical cases. To non-invasively compensate for the aberration in vivo, in-situ aberration correction can be implemented via simulation [43], [44], MR-ARFI [45]–[47], or analytical CT-based methods [44], [48], [52]. Besides, although this system only included the electronic *driving* circuits as our goal for this study was to demonstrate the feasibility of transcranial

MR-guided histotripsy, the receive circuitry can be incorporated into the electronics to enable aberration correction using acquired shockwave signals from acoustic cavitation [49] without dependency on any prior knowledge from CT scans or simulations.

For all measurements and treatments herein, 1-cycle pulses were used to generate cavitation close to the inner skull surface without forming standing waves in the brain. There have been concerns that the pre-focal cavitation at the skull surface may occur when treating close to the skull surface, thus leading to peripheral damage outside of the target volume [32]. With no passive cavitation detector included in the current tcMRgHt system, such concerns were not in the scope of this paper and will be carefully addressed in future investigations.

The tcMRgHt system has demonstrated the capability of generating effective treatment at volume target through the human calvarium and maintaining good MR image quality at the same time. As mentioned in section III.B.1, the cable location had the most significant impact on SNR. The waveguide was originally designed to attenuate the frequency components below its cut-off frequency to prevent external RF interference. When conductors such as cables were introduced in the waveguide, the waveguide became a coaxial cable with no cut-off frequency and allowed noise to enter the scanner room. Conceptually the waveguide should only be used for passing non-metallic accessories like optical fibers, gas hoses, and fluid pipes, whereas any electrical cables should pass the penetration panel via filtered BNC, DB-25, and other connectors on the penetration panel. However, the common commercially available filters only have at most 50 pins, and even if hundreds of pins are available, connecting all channels of the histotripsy system via the filters would be very time-consuming.

We further decomposed the source of noise by calculating the ratio of external interference from the cables through the wall to object noise. When cables were left in the scanner room, the variance σ_1^2 was induced only by the inherent thermal noise. In comparison, when cables were fed through the waveguide, the variance included both inherent thermal noise and the shielding noise through the wall, i.e., $\sigma_2^2 = \sigma_1^2 + \sigma_{wall}^2$. Therefore, $\frac{\sigma_{wall}}{\sigma 1} = \sqrt{\sigma_2^2/\sigma_1^2 - 1} \approx 2.6$, which implies that the noise due to RF shielding through the wall was 2.6 times the inherent thermal noise. Although the standard deviation of pixels was measured in air, which was not the same as that in tissue, the results indicated that improved filtering of the conductors can potentially lead to better image SNR. Once the cables were fed through the waveguide penetration, the SNR was only influenced slightly by the power status, electrical excitation, and acoustic pressure of the tcMRgHt system. We also noted that the operation of the histotripsy array did not produce obvious streaking or other image artifacts. These match well with our intuition, as the resonance frequency of the transducers on the histotripsy array is much lower than the resonance frequency of the 3T scanner (700 kHz compared to 128 MHz), and histotripsy treatment is performed at even lower PRF in a range of 1-200 Hz.

The non-uniformity of B0 and B1 maps measured in this study turned out to be comparable with the non-uniformity that is usually observed in human scans. For B0, Stockmann *et al.* reported an average standard deviation of 31.8 Hz over the head with 2nd order shimming [50], which is better than the standard deviation of 44.8 Hz over the entire map but less than

the standard deviation of 23.4 Hz in ROI in our work, both with first-order shimming only. For B1, the coefficient of variation C_v is typically defined as standard deviation over mean and reported to be 0.2 to 0.27 over larger FOVs for human scans [51], which is on par with the C_v of 0.22 (i.e., 12.9/58.9) on the whole map and 0.23 (i.e., 16/69.1) in ROI in our work.

In general, the image quality achieved in this study was sufficient to demonstrate that ablation was successfully generated during histotripsy treatment. To further demonstrate the treatment outcome and evaluate the treatment safety, the imaging protocols could be optimized to achieve better resolution and SNR by using a larger number of averages, thinner slices, and a smaller FOV, etc. However, changing these parameters will also lead to longer acquisition time and risks of aliasing. More investigation will be done to realize a better trade-off between image quality and other concerns.

As the goal of this study was to develop the first preclinical tcMRgHt system, characterize its performance, and demonstrate the feasibility of MR-guided histotripsy, histopathological analysis on treatment outcomes was not presented here. Potential safety concerns on the in vivo transcranial treatment will be addressed in a different paper. Though the tcMRgHt system presented here was specifically oriented to the preclinical investigation, it provided a realistic prototype for a human-scale tcMRgHt system and shed light on potential improvements for future system design. For clinical translation, we envision a full hemispherical transducer array to be integrated with an acoustic coupler, a stereotactic frame, and an MR-conditional motorized positioner to facilitate the treatment. More details on the development of the clinical tcMRgHt system will be investigated in future studies.

V. Conclusion

This study developed the first preclinical tcMRgHt system for in vivo treatment. A 700-kHz, 128-element MR-compatible phased array was designed and fabricated. Support structures were also designed and constructed to facilitate transcranial treatment. The tcMRgHt array was acoustically characterized with an estimated peak negative pressure up to 137 MPa in free field, 72 MPa through an excised human calvarium with phase aberration correction, and 48.4 MPa through the calvarium without aberration correction. The transcranial focal size of the tcMRgHt array was measured to be slightly larger than that in the free field due to the presence of calvarium. Lesion generation using electronic focal steering only was visualized in a red blood cell agarose phantom, demonstrating a millimeter-level precision of transcranial histotripsy. The electronic focal steering range through the calvarium was 33.5 mm laterally and 50 mm axially, where peak negative pressure above the 26 MPa cavitation intrinsic threshold can be achieved. The MR-compatibility of the tcMRgHt system was assessed quantitatively using SNR, B0 field map, and B1 field map in a clinical 3T MRI scanner. The feasibility of tcMRgHt treatment was demonstrated by successfully generating ablation in the brain of two pigs through the human calvarium with no excessive hemorrhage or edema observed. These results demonstrated the feasibility of using this tcMRgHt system for in vivo transcranial treatment and enabled further investigation on MR-guided histotripsy.

Acknowledgment

The authors would like to thank Aleksandra Rakic from Histosonics Inc. for helping with the design of the transducer scaffold frame and the pig v-tray.

This work was supported by NIH Grant 1R01EB028309 and the Focused Ultrasound Foundation.

Biographies

Ning Lu received the B.S.E. degree (Hons.) from Southeast University, Nanjing, China, in 2018, and the M.S.E degree from the University of Michigan, Ann Arbor, MI, USA, in 2020, both in Biomedical Engineering. She is currently pursuing the Ph.D. degree in Biomedical Engineering and Scientific Computing at the University of Michigan, Ann Arbor. Her research interests include ultrasound instrumentation, transcranial histotripsy, and feedback and monitoring for acoustic therapies. She was a recipient of the Rackham International Student Fellowship from the University of Michigan for 2019-2020.

Timothy L. Hall received his PhD from the University of Michigan, Ann Arbor in 2007. He is one of the original developers of histotripsy ultrasound therapy. His major research interests are in instrumentation for acoustics and lithotripsy and furthering medical applications for histotripsy.

Dave Choi received a B.S.E. degree in mechanical engineering from the University of Michigan, Ann Arbor, MI, USA in 2004. From 2004 to 2006, he was a Research Assistant with the Radiology and Nuclear Medicine Department, University of Michigan Health System, Ann Arbor, MI, USA, and from 2006 to 2013, he was a Product Design Engineer with Honda R&D Americas, Raymond, OH, USA. His main research interests include the design and development of tools and equipment to facilitate biomedical research, particularly equipment designed for PET and MRI compatibility, and ultrasonic therapies such as histotripsy.

Since 2019 he has been a Research Specialist with the Biomedical Engineering Department, University of Michigan College of Engineering, Ann Arbor, MI, USA where he has been assisting with designing and developing tools and equipment for transcranial histotripsy.

Dinank Gupta was born in 1995 in Uttar Pradesh, India. He received the B.S. degree from the Ohio State University, Columbus in 2017 and the M.S. degree from the University of Michigan, Ann Arbor in 2019, both in Electrical Engineering. He is currently pursuing a Ph.D. in Biomedical Engineering from the University of Michigan, Ann Arbor. His research interest is on developing MRI methods for histotripsy treatments, particularly on designing MRI pulse sequence, image acquisition and reconstruction methods for MR-guided histotripsy treatments.

Badih Junior Daou is currently a Neurosurgery Resident at the University of Michigan. He received a Bachelor of Science degree from the University of Balamand, Lebanon in 2010, and an MD degree from the University of Balamand, Lebanon in 2014. He then completed a two-year research fellowship in vascular and endovascular neurosurgery at Thomas Jefferson University (2014-2016), after which he joined the Neurosurgery department at the University of Michigan, Ann Arbor, USA. He is currently a PGY 5 resident at the University of Michigan in the subspecialty of Neurosurgery. His research interests focus on cerebrovascular neurosurgery, intracranial hemorrhage, brain aneurysms and vascular malformations.

Jonathan R. Sukovich received the B.S. and Ph.D. degrees in mechanical engineering from Boston University, Boston, MA, USA, in 2008 and 2013, respectively, where he studied laser interactions with water at high pressures and phenomena associated with high-energy bubble collapse events. He joined the University of Michigan, Ann Arbor, MI, USA, in the summer of 2013 to study histotripsy for brain applications. He is currently an Assistant Research Scientist with the Department of Biomedical Engineering, University of Michigan. His research interests include high-energy bubble collapse phenomena, focused ultrasound therapies, and acoustic cavitation.

Tyler I. Gerhardson received his M.S. and Ph.D. degrees with the Department of Biomedical Engineering at the University of Michigan, Ann Arbor, MI, USA, in 2017 and 2020, respectively. He received a B.S. degree in biomedical engineering from Western New England University, Springfield, MA, USA in 2015. Selected honors include fellowships from Tau Beta Pi and the National Science Foundation Graduate Research Program. Tyler's research interests include ultrasonic standing wave separators, ultrasound transducers and focused ultrasound therapies.

Dr. Aditya S. Pandey, MD , is a Professor of Neurological Surgery and Radiology and specializes in the microsurgical as well as endovascular treatment of cerebrovascular and spinal-vascular pathology. He received his Bachelor of Science in Biological and Engineering Sciences at Washington University in St. Louis and medical training at the Case Western Reserve University. His Neurological Surgery and Cerebrovascular Fellowship training occurred at Thomas Jefferson University Hospital.

Dr. Pandey currently serves as the Surgical Director of the University of Michigan Comprehensive Stroke Center as well as the Director of the Endovascular Neurosurgery Fellowship. He also serves as an associate editor for *Operative Neurosurgery*. His research interests involve the development of histotripsy treatment for brain and spinal cord applications as well as understanding cerebral injury post hemorrhagic stroke including MRI based imaging of cerebral injury and brain iron deposition. Dr. Pandey received the Innovator Grant award from the American Hydrocephalus Association to evaluate the therapeutic potential of acetazolamide in treating hydrocephalus. He is also the Principal Investigator for the DISH Clinical Trial evaluating deferoxamine treatment in those suffering from subarachnoid hemorrhage.

Douglas C. Noll (M '83, SM '12) received his B.S. degree in electrical engineering from Bucknell University, Lewisburg, PA, in 1985, his M.S. and Ph.D. in electrical engineering from Stanford University, Stanford, CA in 1986 and 1991, respectively. From 1985-1987, he was with AT&T Bell Laboratories in Whippany, NJ.

In 1991, he joined the Department of Radiology, University of Pittsburgh, Pittsburgh, PA as an Assistant Professor and later Associate Professor. In 1998, he joined the Departments of Biomedical Engineering and Radiology, University of Michigan, Ann Arbor, MI where he is currently the Ann and Robert H. Lurie Professor of Biomedical Engineering, Professor of Radiology and Co-Director of the Functional MRI Laboratory. He also served as chair of Michigan's Department of Biomedical Engineering from 2006-2013.

Prof. Noll has been performing research in image acquisition, image reconstruction, and functional neuroimaging in MRI for over 30 years. He was the 1994 recipient of the I. I. Rabi Award from the Society of Magnetic Resonance for work in spiral imaging in functional MRI. He is a fellow of the American Institute for Medical and Biological Engineering (AIMBE), the International Society of Magnetic Resonance in Medicine (ISMRM), and the Biomedical Engineering Society (BMES).

Zhen Xu (Member, IEEE) received the B.S.E. degree (Hons.) from Southeast University, Nanjing, China, in 2001, and the M.S. and Ph.D. degrees from the University of Michigan, Ann Arbor, MI, USA, in 2003 and 2005, respectively, all in biomedical engineering. She is currently a Professor of biomedical engineering with the University of Michigan. Her research interests include ultrasound therapy, particularly the applications of histotripsy for non-invasive surgeries.

Dr. Xu received the UFFC Outstanding Paper Award in 2006, the American Heart Association (AHA) Outstanding Research in Pediatric Cardiology in 2010, the National Institute of Health (NIH) New Investigator Award at the First National Institute of Biomedical Imaging and Bioengineering (NIBIB) Edward C. Nagy New Investigator Symposium in 2011, the Frederic Lizzi Early Career Award from ISTU in 2015, the Fellow of American Institute of Medicine and Bioengineering in 2019, and The Lockhart Memorial Prize for Cancer Research in 2020. She is also an Associate Editor of the IEEE Transactions on Ultrasonics, Ferroelectrics, And Frequency Control (UFFC) and BME Frontiers, the Deputy Vice President of the Ultrasonics Standing Committee (USSC) of UFFC, and a Board Member of the International Society of Therapeutic Ultrasound (ISTU).

References

[1]. Aubry JF and Tanter M, "MR-guided transcranial focused ultrasound," Adv. Exp. Med. Biol, vol. 880, pp. 97–111, 2016. [PubMed: 26486334]

[2]. Federau C, Goubran M, Rosenberg J, Henderson J, Halpern CH, Santini V, Wintermark M, Pauly KB, and Ghanouni P, "Transcranial MRI-guided high-intensity focused ultrasound for treatment of essential tremor: A pilot study on the correlation between lesion size, lesion location, thermal dose, and clinical outcome," J. Magn. Reson. Imaging, vol. 48, no. 1, pp. 58–65, 7. 2018, doi: 10.1002/jmri.25878. [PubMed: 29076274]

[3]. Elias WJ, Huss D, Voss T, Loomba J, Khaled M, Zadicario E, Frysinger RC, Sperling SA, Wylie S, Monteith SJ, Druzgal J, Shah BB, Harrison M, and Wintermark M, "A Pilot Study of Focused Ultrasound Thalamotomy for Essential Tremor," N. Engl. J. Med, vol. 369, no. 7, pp. 640–648, 8. 2013, doi: 10.1056/NEJMoa1300962. [PubMed: 23944301]

[4]. Lipsman N, Schwartz ML, Huang Y, Lee L, Sankar T, Chapman M, Hynynen K, and Lozano AM, "MR-guided focused ultrasound thalamotomy for essential tremor: A proof-of-concept study," The Lancet Neurology, vol. 12, no. 5, pp. 462–468, 5 2013, doi: 10.1016/S1474-4422(13)70048-6. [PubMed: 23523144]

[5]. Coluccia D, Fandino J, Schwyzer L, O'Gorman R, Remonda L, Anon J, Martin E, and Werner B, "First noninvasive thermal ablation of a brain tumor with MR-guided focused ultrasound," J. Ther. Ultrasound, vol. 2, no. 1, 2014, doi: 10.1186/2050-5736-2-17.

[6]. Monteith SJ, Kassell NF, Goren O, and Harnof S, "Transcranial MR-guided focused ultrasound sonothrombolysis in the treatment of intracerebral hemorrhage," Neurosurgical Focus, vol. 34, no. 5, 5 2013, doi: 10.3171/2013.2.FOCUS1313.

[7]. Lipsman N, Meng Y, Bethune AJ, Huang Y, Lam B, Masellis M, Herrmann N, Heyn C, Aubert I, Boutet A, Smith GS, Hynynen K, and Black SE, "Blood-brain barrier opening in Alzheimer's disease using MR-guided focused ultrasound," Nat. Commun, vol. 9, no. 1, 12. 2018, doi: 10.1038/s41467-018-04529-6.

[8]. Martin E, Jeanmonod D, Morel A, Zadicario E, and Werner B, "High-intensity focused ultrasound for noninvasive functional neurosurgery," Ann. Neurol, vol. 66, no. 6, pp. 858–861, 12. 2009, doi: 10.1002/ana.21801. [PubMed: 20033983]

[9]. McDannold N, Clement G, Black P, Jolesz F, and Hynynen K, "Transcranial MRI-guided focused ultrasound surgery of brain tumors: Initial findings in three patients," Neurosurgery, vol. 66, no. 2, pp. 323–332, 2010, doi: 10.1227/01.NEU.0000360379.95800.2F.Transcranial. [PubMed: 20087132]

[10]. Ji R, Smith M, Niimi Y, Karakatsani ME, Murillo MF, Jackson-Lewis V, Przedborski S, and Konofagou EE, "Focused ultrasound enhanced intranasal delivery of brain derived neurotrophic factor produces neurorestorative effects in a Parkinson's disease mouse model," Sci. Rep, vol. 9, no. 1, 12. 2019, doi: 10.1038/s41598-019-55294-5.

[11]. Fasano A, De Vloo P, Llinas M, Hlasny E, Kucharczyk W, Hamani C, and Lozano AM, "Magnetic Resonance Imaging-Guided Focused Ultrasound Thalamotomy in Parkinson Tremor: Reoperation After Benefit Decay," Mov. Disord, vol. 33, no. 5, pp. 848–849, 5 2018, doi: 10.1002/mds.27348. [PubMed: 29570865]

[12]. Arvanitis CD, Vykhodtseva N, Jolesz F, Livingstone M, and McDannold N, "Cavitation-enhanced nonthermal ablation in deep brain targets: Feasibility in a large animal model," J. Neurosurg, vol. 124, no. 5, pp. 1450–1459, 5 2016, doi: 10.3171/2015.4.JNS142862. [PubMed: 26381252]

[13]. Pulkkinen A, Huang Y, Song J, and Hynynen K, "Simulations and measurements of transcranial low-frequency ultrasound therapy: Skull-base heating and effective area of treatment," Phys. Med. Biol, vol. 56, no. 15, pp. 4661–4683, 8. 2011, doi: 10.1088/0031-9155/56/15/003. [PubMed: 21734333]

[14]. Xu Z, Fowlkes JB, Rothman ED, Levin AM, and Cain CA, "Controlled ultrasound tissue erosion: The role of dynamic interaction between insonation and microbubble activity," J. Acoust. Soc. Am, vol. 117, p. 424, 2005, doi: 10.1121/1.1828551. [PubMed: 15704435]

[15]. Parsons JE, Cain CA, Abrams GD, and Fowlkes JB, "Pulsed cavitational ultrasound therapy for controlled tissue homogenization," Ultrasound Med. Biol, vol. 32, no. 1, pp. 115–129, 1. 2006, doi: 10.1016/j.ultrasmedbio.2005.09.005. [PubMed: 16364803]

[16]. Khokhlova VA, Fowlkes JB, Roberts WW, Schade GR, Xu Z, Khokhlova TD, Hall TL, Maxwell AD, Wang YN, and Cain CA, "Histotripsy methods in mechanical disintegration of tissue: Towards clinical applications," Int. J. Hyperth, vol. 31, no. 2. Informa Healthcare, pp.145–162, 3. 01, 2015, doi: 10.3109/02656736.2015.1007538.

[17]. Kim Y, Hall T, Xu Z, and Cain C, "Transcranial histotripsy therapy: A feasibility study," IEEE Trans. Ultrason. Ferroelectr. Freq. Control, vol. 61, no. 4, pp. 582–593, 2014, doi: 10.1109/TUFFC.2014.2947.

[18]. Sukovich JR, Xu Z, Kim Y, Cao H, Nguyen TS, Pandey AS, Hall TL, and Cain CA, "Targeted Lesion Generation Through the Skull Without Aberration Correction Using Histotripsy," IEEE Trans. Ultrason. Ferroelectr. Freq. Control, vol. 63, no. 5, pp. 671–682, 5 2016, doi: 10.1109/TUFFC.2016.2531504. [PubMed: 26890732]

[19]. Gerhardson T, Sukovich JR, Pandey AS, Hall TL, Cain CA, and Xu Z, "Effect of Frequency and Focal Spacing on Transcranial Histotripsy Clot Liquefaction, Using Electronic Focal Steering," Ultrasound Med. Biol, vol. 43, no. 10, pp. 2302–2317, 2017, doi: 10.1016/j.ultrasmedbio.2017.06.010. [PubMed: 28716432]

[20]. Eames MDC, Hananel A, Snell JW, Kassell NF, and Aubry JF, "Transcranial focused ultrasound without hair shaving: Feasibility study in an ex vivo cadaver model," J. Ther. Ultrasound, vol. 1, no. 1, 1. 2014, doi: 10.1186/2050-5736-1-24.

[21]. Sukovich JR, Cain CA, Pandey AS, Chaudhary N, Camelo-Piragua S, Allen SP, Hall TL, Snell J, Xu Z, Cannata JM, Teofilovic D, Bertolina JA, Kassell N, and Xu Z, "In vivo histotripsy brain treatment," J. Neurosurg, vol. 131, no. 4, pp. 1331–1338, 10. 2019, doi: 10.3171/2018.4.JNS172652.

[22]. Vlaisavljevich E, Kim Y, Allen S, Owens G, Pelletier S, Cain C, Ives K, and Xu Z, "Image-guided non-invasive ultrasound liver ablation using histotripsy: Feasibility study in an in vivo porcine model," Ultrasound Med. Biol, vol. 39, no. 8, pp. 1398–1409, 2013, doi: 10.1016/j.ultrasmedbio.2013.02.005. [PubMed: 23683406]

[23]. Wang TY, Xu Z, Winterroth F, Fowlkes JB, Hall TL, Roberts WW, Rothman ED, and Cain CA, "Quantitative Ultrasound Backscatter for Pulsed Cavitational Ultrasound Therapy—Histotripsy," IEEE Trans. Ultrason. Ferroelectr. Freq. Control, vol. 56, no. 5, pp. 995–1005, 2009, doi: 10.1109/TUFFC.2009.1131. [PubMed: 19750596]

[24]. Allen SP, Hall TL, Cain CA, and Hernandez-Garcia L, "Controlling cavitation-based image contrast in focused ultrasound histotripsy surgery," Magn. Reson. Med, vol. 73, no. 1, pp. 204–213, 2015, doi: 10.1002/mrm.25115. [PubMed: 24469922]

[25]. Allen SP, Hernandez-Garcia L, Cain CA, and Hall TL, "MR-based detection of individual histotripsy bubble clouds formed in tissues and phantoms," Magn. Reson. Med, vol. 76, no. 5, pp. 1486–1493, 2016, doi: 10.1002/mrm.26062. [PubMed: 26599823]

[26]. Federau C, Goubran M, Rosenberg J, Henderson J, Halpern CH, Santini V, Wintermark M, Pauly KB, Ghanouni P, "Transcranial MRI-guided high-intensity focused ultrasound for treatment of essential tremor: A pilot study on the correlation between lesion size, lesion location, thermal dose, and clinical outcome," J. Magn. Reson. Imaging, vol. 48, no. 1, pp. 58–65, 7. 2018, doi: 10.1002/jmri.25878. [PubMed: 29076274]

[27]. Payne A, Minalga E, Merrill R, Parker DL, and Hadley JR, "Technical Note: Effect of transducer position and ground plane configuration on image quality in MR-guided focused ultrasound therapies," Med. Phys, vol. 47, no. 6, pp. 2350–2355, 6. 2020, doi: 10.1002/mp.14138. [PubMed: 32170866]

[28]. Gerhardson T, "Transcranial Therapy for Intracerebral Hemorrhage and Other Brain Pathologies using Histotripsy," Ph.D. dissertation, University of Michigan, Ann Arbor, MI, 2020.

[29]. Cohen ZR, Zaubermann J, Harnof S, Mardor Y, Nass D, Zadicario E, Hananel A, Castel D, Faibel M, and Ram Z, "Magnetic resonance imaging-guided focused ultrasound for thermal ablation in the brain," Neurosurgery, vol. 60, no. 4, pp. 593–600, 4. 2007, doi: 10.1227/01.NEU.0000245606.99946.C6. [PubMed: 17415195]

[30]. Alkins R, Huang Y, Pajek D, and Hynynen K, "Cavitation-based third ventriculostomy using MRI-guided focused ultrasound: Laboratory investigation," J. Neurosurg, vol. 119, no. 6, pp. 1520–1529, 12. 2013, doi: 10.3171/2013.8.JNS13969. [PubMed: 24074494]

[31]. Huang Y, Alkins R, Schwartz ML, and Hynynen K, "Opening the Blood-Brain Barrier with MR Imaging–guided Focused Ultrasound: Preclinical Testing on a Trans–Human Skull Porcine Model," Radiology, vol. 282, no. 1, pp. 123–130, 1. 2017, doi: 10.1148/radiol.2016152154. [PubMed: 27420647]

[32]. O'Reilly MA, Huang Y, and Hynynen K, "The impact of standing wave effects on transcranial focused ultrasound disruption of the blood-brain barrier in a rat model," Phys. Med. Biol, vol. 55, no. 18, pp. 5251–5267, 9. 2010, doi: 10.1088/0031-9155/55/18/001. [PubMed: 20720286]

[33]. Lechner-Greite SM, Hehn N, Werner B, Zadicario E, Tarasek M, and Yeo D, “Minimizing eddy currents induced in the ground plane of a large phased-array ultrasound applicator for echo-planar imaging-based MR thermometry,” J. Ther. Ultrasound, vol. 4, no. 1, p. 4, 12. 2016, doi: 10.1186/s40349-016-0047-x. [PubMed: 26848391]

[34]. Fry FJ and Barger JE, “Acoustical properties of the human skull,” J. Acoust. Soc. Am, vol. 63, no. 5, pp. 1576–1590, 5 1978, doi: 10.1121/1.381852. [PubMed: 690336]

[35]. Pinton G, Aubry JF, Bossy E, Muller M, Pernot M, and Tanter M, “Attenuation, scattering, and absorption of ultrasound in the skull bone,” Med. Phys, vol. 39, no. 1, pp. 299–307, 2012, doi: 10.1118/1.3668316. [PubMed: 22225300]

[36]. Parsons JE, Cain CA, and Fowlkes JB, “Cost-effective assembly of a basic fiber-optic hydrophone for measurement of high-amplitude therapeutic ultrasound fields,” J. Acoust. Soc. Am, vol. 119, no. 3, pp. 1432–1440, 2006, doi: 10.1121/1.2166708. [PubMed: 16583887]

[37]. Maxwell AD, Cain CA, Hall TL, Fowlkes JB, and Xu Z, “Probability of cavitation for single ultrasound pulses applied to tissues and tissue-mimicking materials.,” Ultrasound Med. Biol, vol. 39, no. 3, pp. 449–65, 3. 2013, doi: 10.1016/j.ultrasmedbio.2012.09.004. [PubMed: 23380152]

[38]. Gateau J, Aubry JF, Chauvet D, Boch AL, Fink M, and Tanter M, “In vivo bubble nucleation probability in sheep brain tissue,” Phys. Med. Biol, vol. 56, no. 22, pp. 7001–7015, 11. 2011, doi: 10.1088/00319155/56/22/001. [PubMed: 22015981]

[39]. Maxwell AD, Wang TY, Yuan L, Duryea AP, Xu Z, and Cain CA, “A tissue phantom for visualization and measurement of ultrasound-induced cavitation damage,” Ultrasound Med. Biol, vol. 36, no. 12, pp. 2132–2143, 12. 2010, doi: 10.1016/j.ultrasmedbio.2010.08.023. [PubMed: 21030142]

[40]. Insko EK and Bolinger L, “Mapping of the radiofrequency field,” J. Magn. Reson, vol. 103, no. 1, pp. 82–85, 6. 1993, doi: 10.1006/jmra.1993.1133.

[41]. Jezzard P and Balaban RS, “Correction for geometric distortion in echo planar images from B0 field variations,” Magn. Reson. Med, vol. 34, no. 1, pp. 65–73, 1995, doi: 10.1002/mrm.1910340111. [PubMed: 7674900]

[42]. Cunningham CH, Pauly JM, and Nayak KS, “Saturated double-angle method for rapid B1+ mapping,” Magn. Reson. Med, vol. 55, no. 6, pp. 1326–1333, 6. 2006, doi: 10.1002/mrm.20896. [PubMed: 16683260]

[43]. Leung SA, Webb TD, Bitton RR, Ghanouni P, and Pauly KB, “A rapid beam simulation framework for transcranial focused ultrasound,” Sci. Rep, vol. 9, no. 1, pp. 1–11, 12. 2019, doi: 10.1038/s41598-019-43775-6. [PubMed: 30626917]

[44]. Jones RM and Hynynen K, “Comparison of analytical and numerical approaches for CT-based aberration correction in transcranial passive acoustic imaging,” Phys. Med. Biol, vol. 61, no. 1, pp. 23–36, 11. 2015, doi: 10.1088/0031-9155/61/1/23. [PubMed: 26605827]

[45]. Miller GW, Eames M, Snell J, and Aubry JF, “Ultrashort echo-time MRI versus CT for skull aberration correction in MR-guided transcranial focused ultrasound: In vitro comparison on human calvaria,” Med. Phys, vol. 42, no. 5, pp. 2223–2233, 5 2015, doi: 10.1118/1.4916656. [PubMed: 25979016]

[46]. Vyas U, Kaye E, and Pauly KB, “Transcranial phase aberration correction using beam simulations and MR-ARFI,” Med. Phys, vol. 41, no. 3, p. 032901, 3. 2014, doi: 10.1118/1.4865778. [PubMed: 24593740]

[47]. Liu N, Liutkus A, Aubry J-F, Marsac L, Tanter M, and Daudet L, “Random calibration for accelerating MR-ARFI guided ultrasonic focusing in transcranial therapy.,” Phys. Med. Biol, vol. 60, no. 3, pp. 106–985, 2. 2015, doi: 10.1088/0031-9155/60/3/1069.

[48]. Jones RM, O’Reilly MA, and Hynynen K, “Experimental demonstration of passive acoustic imaging in the human skull cavity using CT-based aberration corrections,” Med. Phys, vol. 42, no. 7, pp. 4385–4400, 7. 2015, doi: 10.1118/1.4922677. [PubMed: 26133635]

[49]. Macoskey JJ, Hall TL, Sukovich JR, Choi SW, Ives K, Johnsen E, Cain CA, and Xu Z. “Soft-Tissue Aberration Correction for Histotripsy,” IEEE Trans. Ultrason. Ferroelectr. Freq. Control, vol. 65, no. 11, pp. 2073–2085, 11. 2018, doi: 10.1109/TUFFC.2018.2872727. [PubMed: 30281443]

[50]. Stockmann JP, Witzel T, Keil B, Polimeni JR, Mareyam A, Lapierre C, Setsompop K, and Wald LL, “A 32-channel combined RF and B0 shim array for 3T brain imaging,” Magn. Reson. Med, vol. 75, no. 1, pp. 441–451, 1. 2016, doi: 10.1002/mrm.25587. [PubMed: 25689977]

[51]. Childs AS, Malik SJ, O’Regan DP, and Hajnal JV, “Impact of number of channels on RF shimming at 3T,” Magnetic Resonance Materials in Physics, Biology and Medicine, vol. 26, no. 4, pp. 401–410, 8. 2013, doi: 10.1007/s10334-012-0360-5.

[52]. Alkins R, Huang Y, Pajek D, and Hynynen K, “Cavitation-based third ventriculostomy using MRI-guided focused ultrasound: Laboratory investigation,” J. Neurosurg, vol. 119, no. 6, pp. 1520–1529, 12. 2013, doi: 10.3171/2013.8.JNS13969. [PubMed: 24074494]

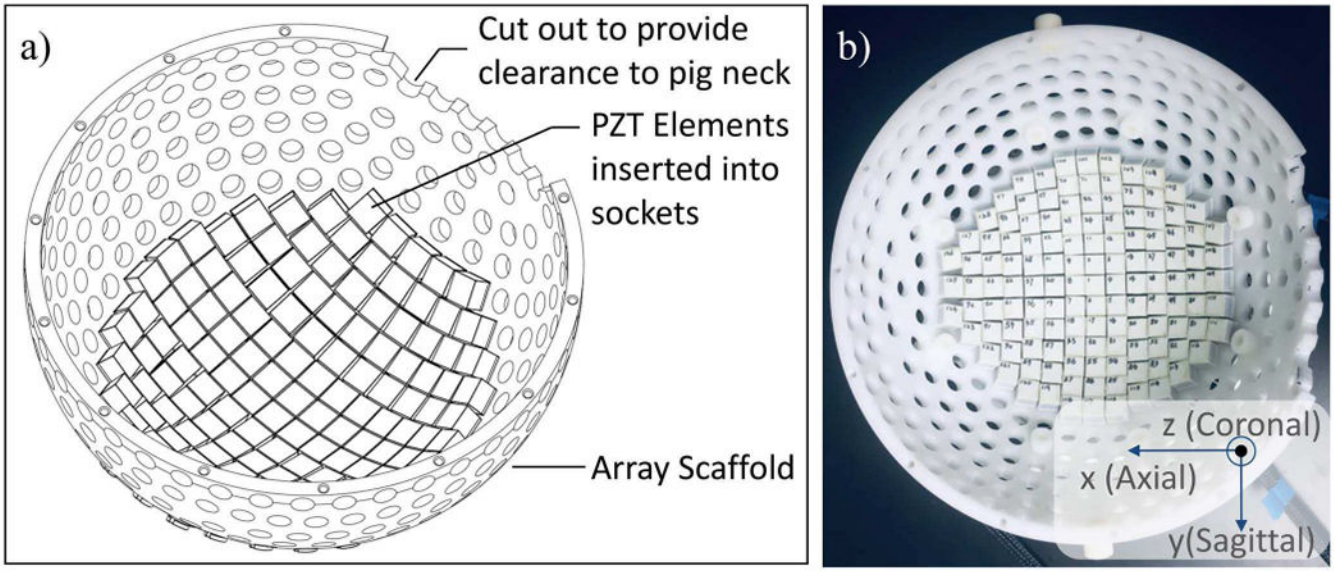

Fig. 1.

The schematic drawing (a) and photo (b) of the 128-element MR-compatible histotripsy array. The coordinate system in b is defined according to directions in the MR scanner.

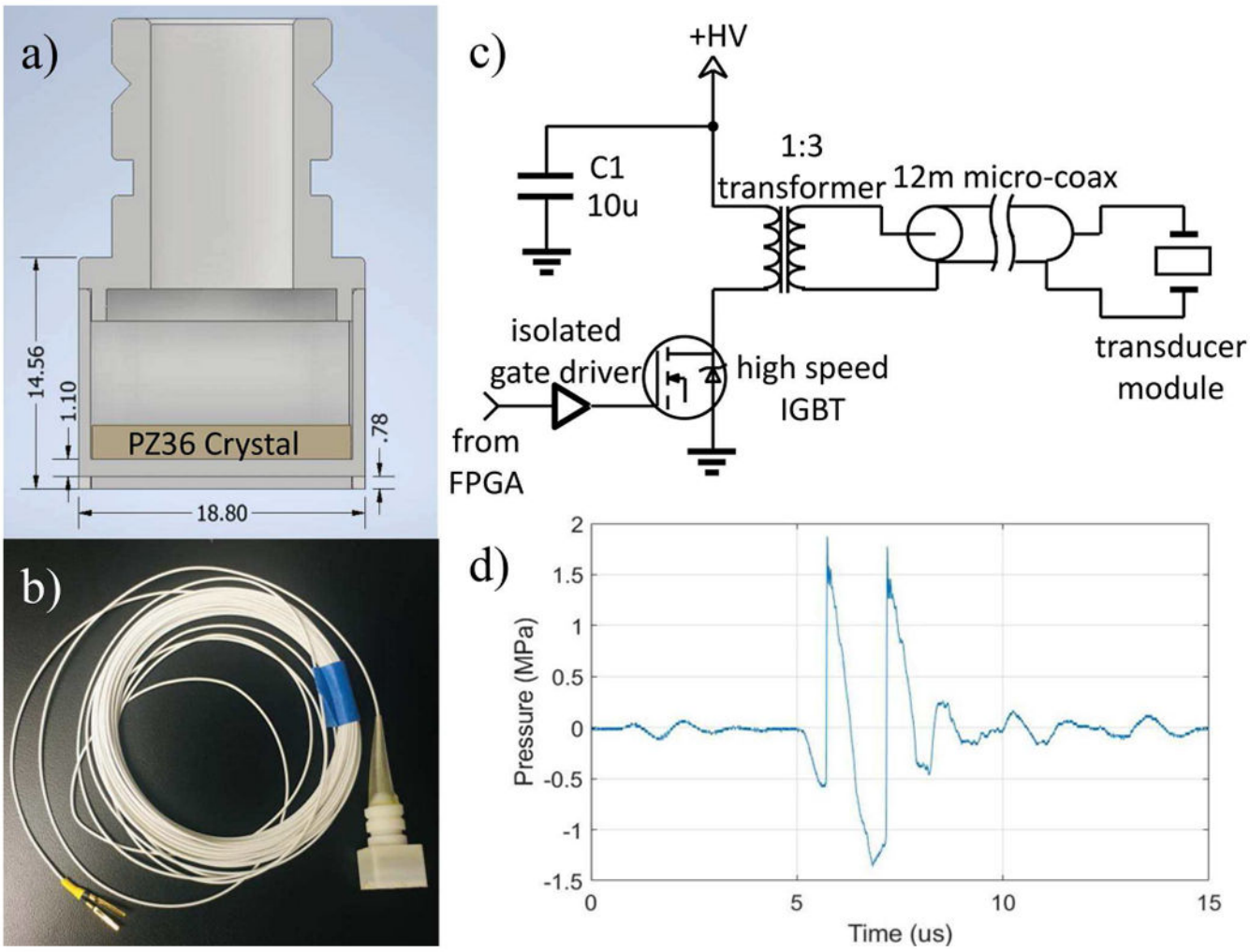

Fig. 2.

Single transducer module for the tcMRgHt array. a): Cross-section of the transducer module design. The PZ36 crystal is labeled in the figure. Two matching layers were placed in front of the crystal for impedance matching. Dimensions are in the unit of mm. b): Photo of a single transducer module with 11-meter coaxial cable. c): Schematic of the driving circuitry for a single transducer module. d): The pressure waveform produced from a single module at 150 mm in the free field with a drive voltage of 3.5 kV. The peak negative pressure was measured to be 1.36 MPa.

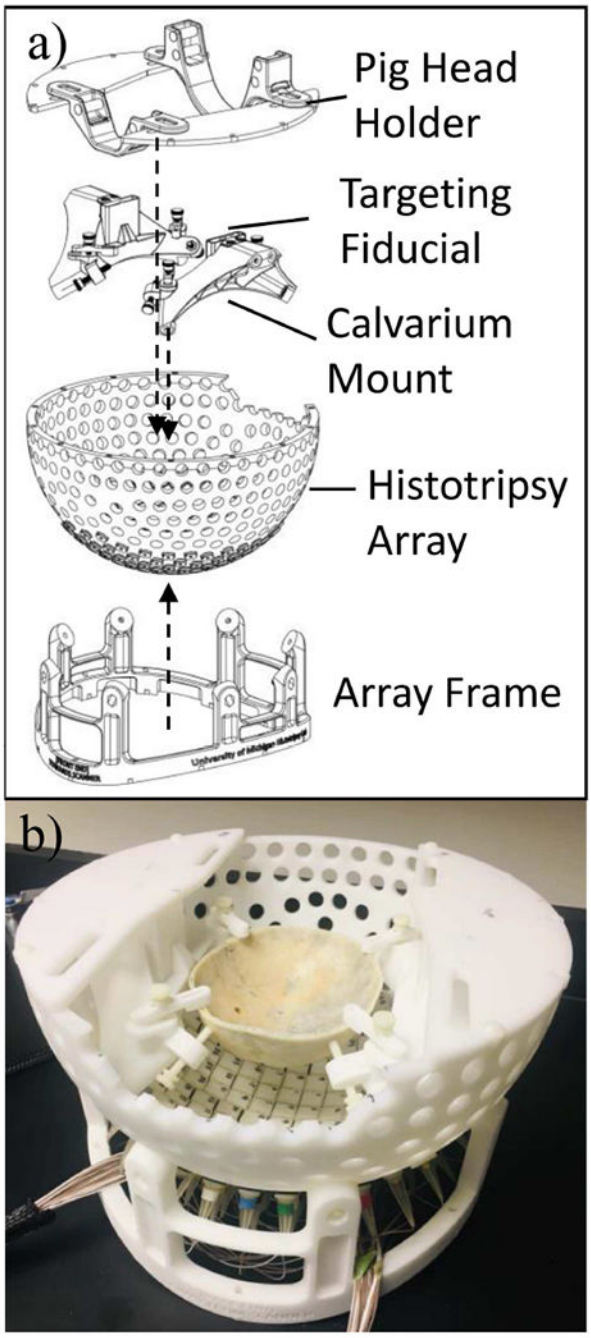

Fig. 3.
Exploded view (a) and photo (b) of the tcMRgHt array and accessories.

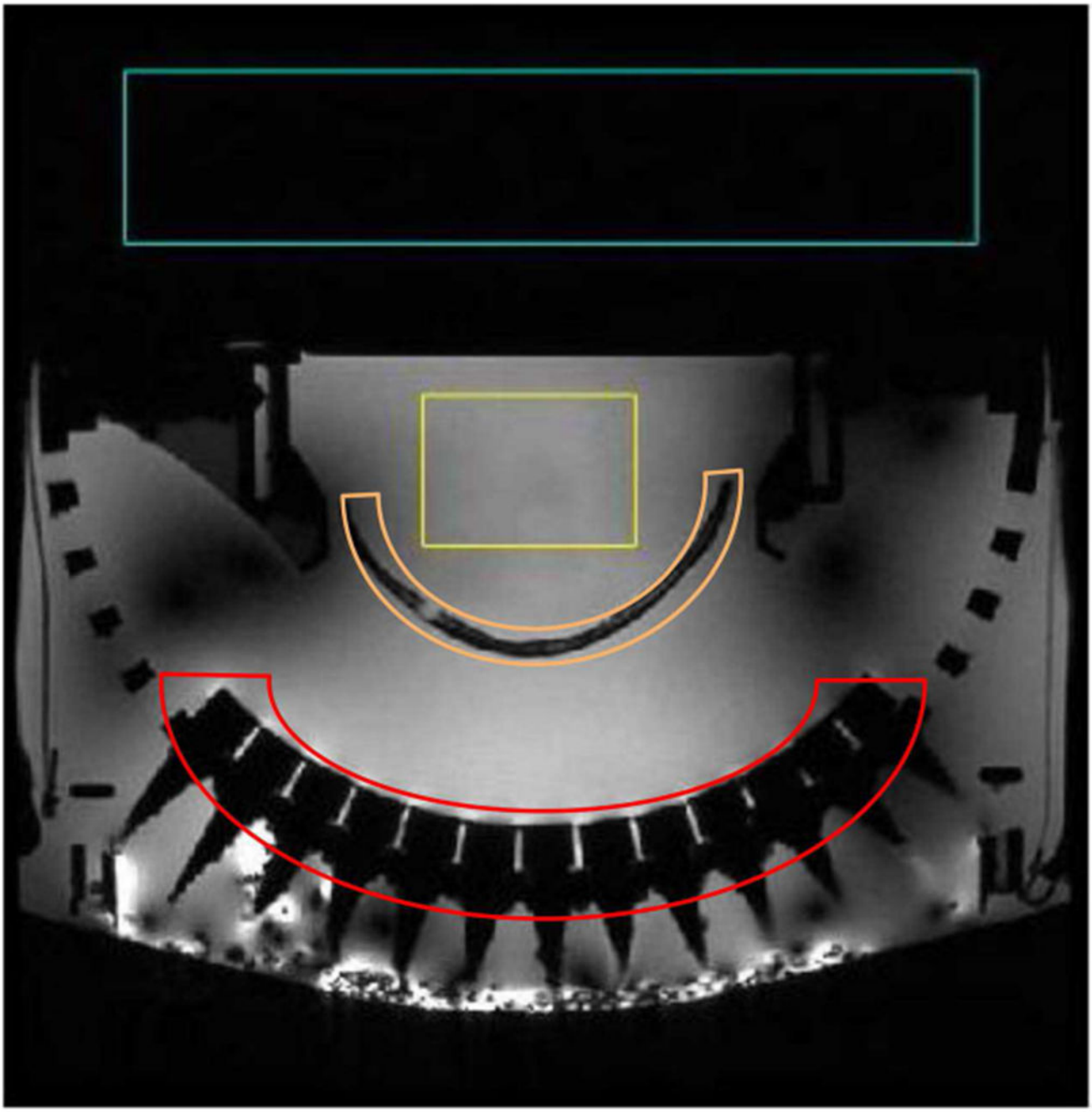

Fig. 4.
An example of magnitude images from SNR measurement. The signal region (yellow) and background region (blue) used for SNR measurement are shown in the image. The excised calvarium and ultrasound transducers are labeled as orange and red, respectively.

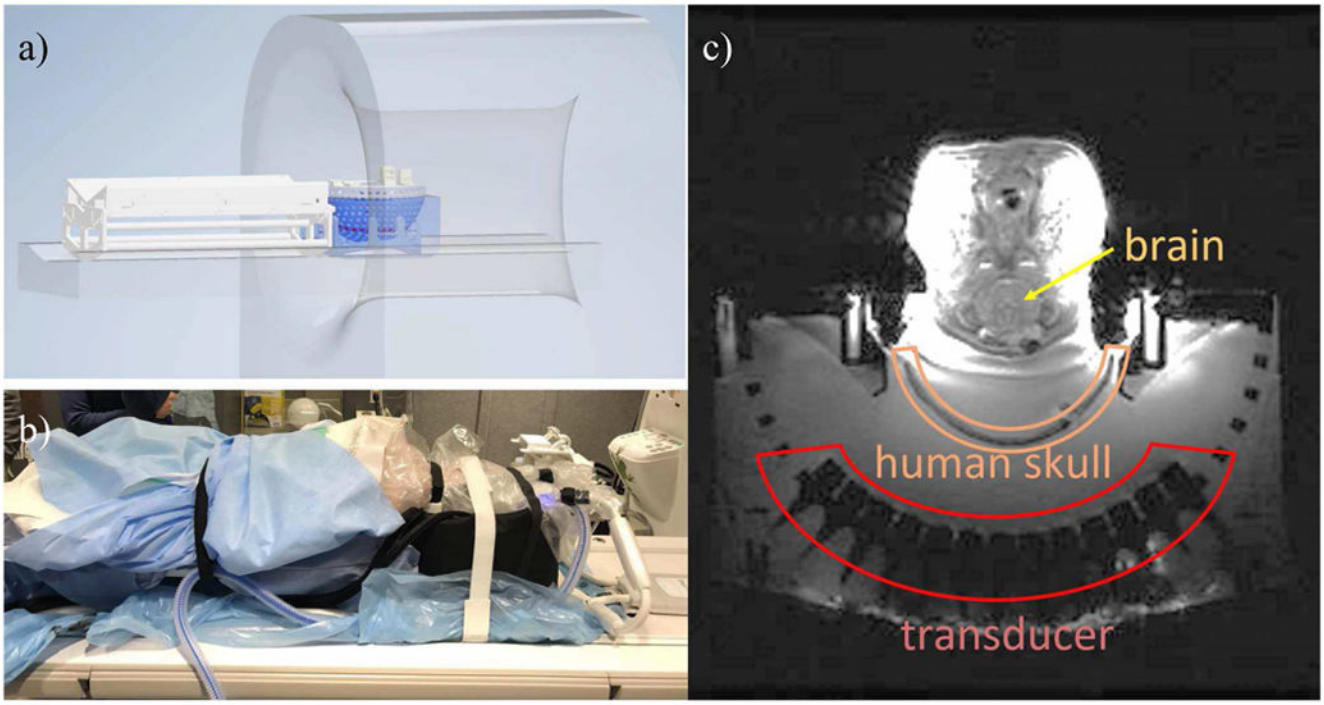

Fig. 5.

Diagram (a) and photo (b) of the experimental setup for in vivo pig treatment. With the tcMRgHt system placed on the MR bed, the pig was placed supine on a v-tray with its head supported by the snout and neck holder on the tcMRgHt system. An MR image on the transverse plane (c) demonstrated the locations of transducer elements, the human skull, and the pig brain.

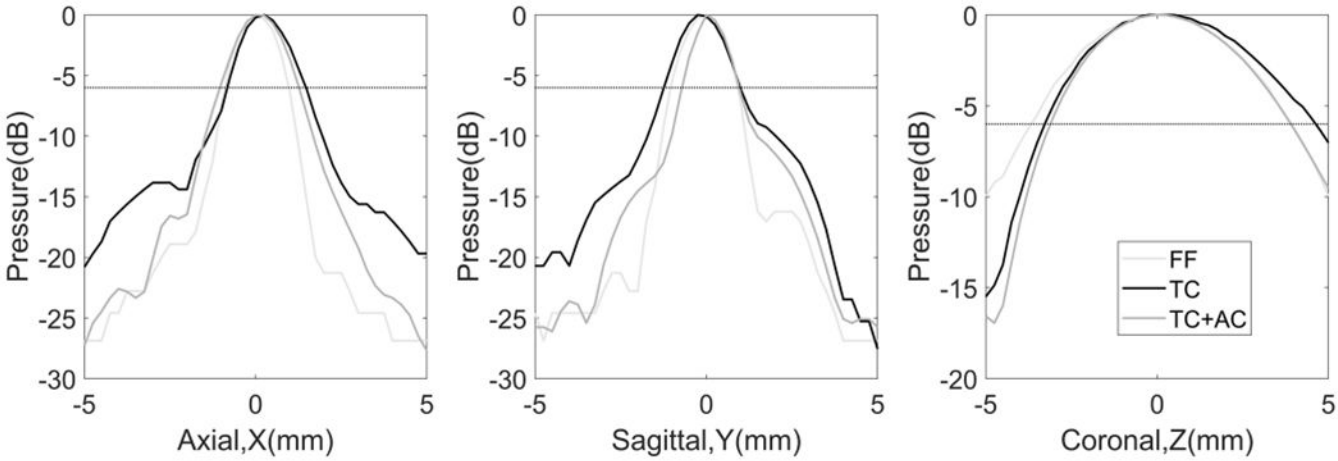

Fig. 6.

Normalized beam profiles of the tcMRgHt array. FF: free field (light gray); TC: through the human skull (black); TC+AC: through the human skull with phase aberration correction (dark gray). The dotted horizontal line at −6 dB indicated half of the maximum pressure, so the FWHM was the distance between the two locations where −6 dB was achieved on each profile.

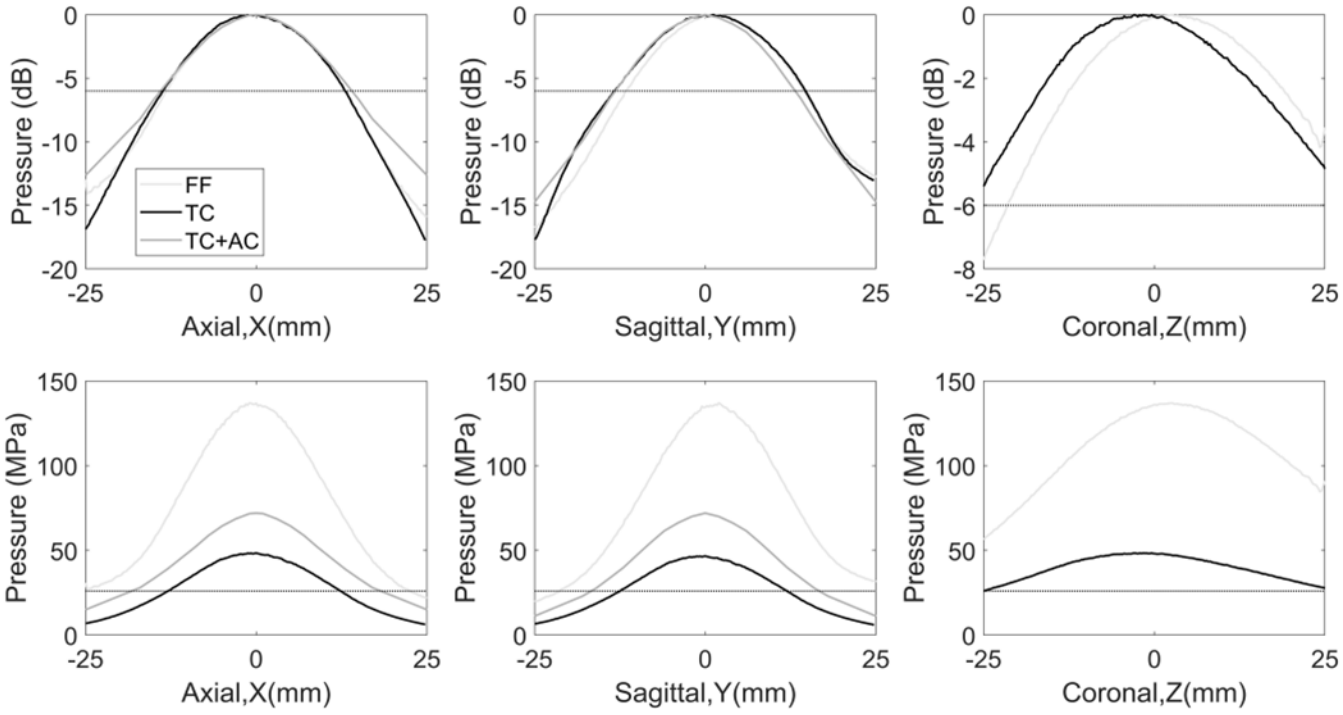

Fig. 7.

Steering profiles of the tcMRgHt array. FF: free field (light gray); TC: through the human skull (black); TC+AC: through the human skull with phase aberration correction (dark gray). Top row: Normalized steering profiles scaled to dB relative to the maximum pressure in each case, where the −6 dB line was labeled to indicate the −6 dB steering range. Bottom row: The steering profiles in absolute P- values, where the 26 MPa cavitation intrinsic threshold was labeled to indicate the effective therapeutic range.

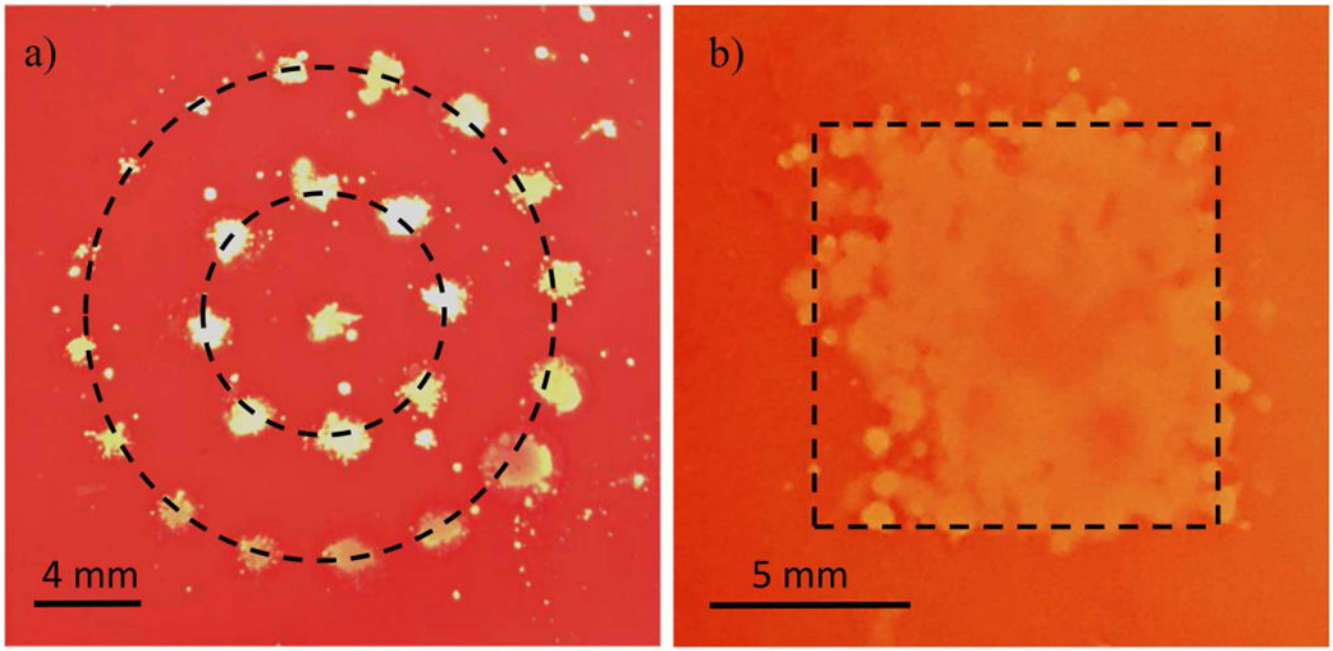

Fig. 8.

Histotripsy ablation generated by electronic focal steering in the RBC phantom. a): Sparse circular pattern centered at the geometric focus. b): A 10-mm continuous square lesion representing a volume ablation zone in the transverse plane.

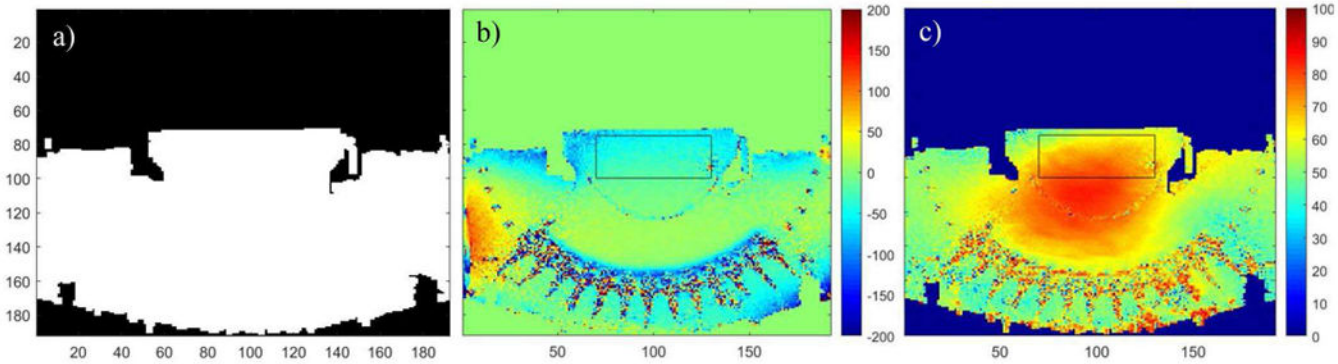

Fig. 9.

B0 and B1 field maps for tcMRgHt experiments. a): The binary mask applied to reconstructed field maps. b): B0 field map for off-resonance in Hz. c): B1 field map for actual tip angle.

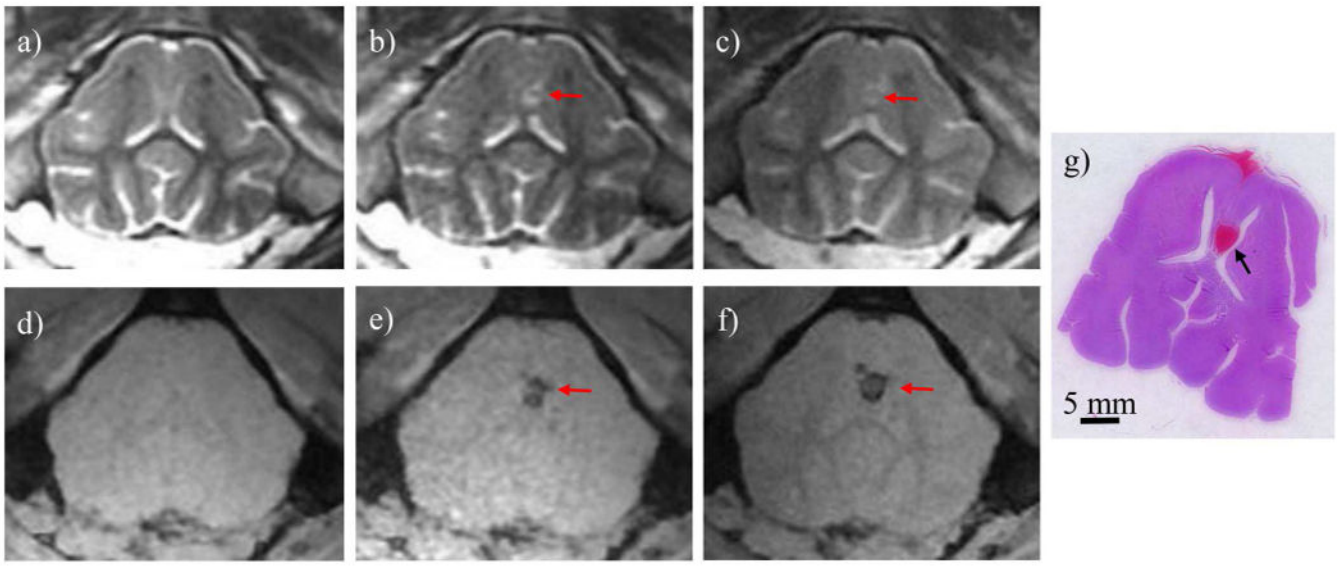

Fig. 10.

MR images and histology slice from one treated pig brain. T2-weighted scans (a-c) showed a hyperintense ablation zone immediately after treatment (b) and 2 hours post-treatment (c), compared to the pre-treatment image (a). T2*-weighted scans (d-f) showed hypointense ablation zone on the immediately after treatment (e) and 2 hours post-treatment (f), compared to pre-treatment image (d). A Hematoxylin and Eosin (H&E) stained slice (g) showed an ablation zone adjacent to the ventricles corresponding to the MR images. The hemorrhage on the base of the brain was because the RBCs from the treated zone flowed through the longitudinal fissure and was not associated with histotripsy damage.

TABLE I

MEASURED PRESSURE, FOCAL SIZE, AND STEERING RANGE.

	Maximal Focal Pressure (MPa)	Focal Size (mm^3)	Steering Range Metric	Electronic Steering Range		
				X (mm)	Y (mm)	Z (mm)
FF	137	1.9×2×7.6	−6 dB	26.5	26.5	>50
			>26 MPa	47.5	50	>50
TC+AC	72	2.2×1.7×7	−6 dB	28	27	>50
			>26 MPa	37	33.5	>50
TC	48.4	2.3×2.2×7.9	−6 dB	27	28.25	>50
			>26 MPa	25.25	24.5	>50

FF: free field; TC+AC: through the skull with aberration correction; TC: through the skull without aberration correction.